Response of high-energy protons of the inner radiation belt to large magnetic storms

Hong Zou,[1,2] Qiu Gang Zong,[1,3] George K. Parks,[2] Zu Yin Pu,[1] Hong Fei Chen,[1] and Lun Xie[1]

Received 11 April 2011; revised 9 August 2011; accepted 10 August 2011; published 26 October 2011.

[1] The responses of the high-energy protons (35–70 MeV, 70–140 MeV and 140–500 MeV) below L = 3 to the large geomagnetic magnetic storms (|Dst| > 200 nT) during 1998 to 2005 have been investigated with the measurements by three NOAA POES satellites (NOAA-15, 16 and 17). The losses of protons in the outer region of the inner radiation belt are found during the large storms. Similar loss events were also measured by the HEO-3 satellite for lower energy protons (8.5–35 MeV, 16–40 MeV and 27–45 MeV). However, the response of higher energy protons to the storms observed by NOAA satellites is different from that of the lower energy protons. It is shown that some aspects of the loss event and energy dependence during large storms can be accounted for by the trapping limit of the field line curvature scattering mechanism. The maximal L shells of the observed trapped protons are consistent with the critical L shells of the field line curvature scattering. The modeling results based on the storm-time geomagnetic field model (TS04c) and the radiation belt model (AP8) show the inward motion of the outer boundary of trapped protons is caused by the distortion of geomagnetic field during the magnetic storms and depends on proton energy. The additional proton loss in the lower energy channel (35–70 MeV) could be attributed to the storm-caused weakening of geomagnetic field combined with L dependent lifetimes induced by curvature scattering during magnetic storms.

Citation: Zou, H., Q. G. Zong, G. K. Parks, Z. Y. Pu, H. F. Chen, and L. Xie (2011), Response of high-energy protons of the inner radiation belt to large magnetic storms, *J. Geophys. Res.*, *116*, A10229, doi:10.1029/2011JA016733.

1. Introduction

[2] To understand the dynamics of high-energy particles in the radiation belts is of great importance from both practical and space physics points of view. There are many studies of the radiation belt particles. The hot topics in the radiation belt research are mainly about the outer belt dynamics. It is known that the electrons in the outer radiation belt (3 < L < 7) show large variations in both space and time, especially during strong geomagnetic activity [*Dessler and Karplus*, 1961; *Baker et al.*, 1999; *Li et al.*, 1997; *Kim and Chan*, 1997; *Reeves et al.*, 1998; *Li et al.*, 2001; *Miyoshi et al.*, 2003]. A new belt of relativistic electrons in the inner radiation belt (L < 2) has also been reported to form following the large storms that occurred during the years 2003–2005 [*Looper et al.*, 2005; *Baker et al.*, 2007].

[3] Compared to the electrons, the inner radiation belt protons are more stable, varying mainly with the 11-year solar activity cycle [*Li et al.*, 2001]. However, the short-term variations of the inner radiation belt gained more attention recently as some studies showed that strong geomagnetic disturbance effects can reach to very low L values. A sudden injection inside L = 3 of electrons and protons with energies up to tens of MeV was reported during the period of the strong geomagnetic activity in late March 1991 [*Blake et al.*, 1992]. With the measurements of the Solar, Anomalous, and Magnetospheric Particle Explorer (SAMPEX), *Looper et al.* [2005] found that the protons in the two energy ranges of 19–29 MeV and 86–120 MeV around L = 2 almost completely disappeared during the famous Halloween events from late October to early November 2003. Similar events could not be found in the entire SAMPEX mission before October 2003.

[4] *Selesnick et al.* [2010] recently found additional loss events from a long-term measurement by HEO-3 satellite from 1998 to 2005, in which low energy protons in the outer region of the inner radiation belt (L = 2 to 3) disappeared during large geomagnetic storms. The L ranges for the loss events were correlated with the minimum Dst for Dst < −100 nT. Moreover, the radial extent of loss events reached inward of L = 2 and the inner locations were energy independent for three channels (8.5–35 MeV, 16–40 MeV and 27–45 MeV). The

[1]School of Earth and Space Sciences, Peking University, Beijing, China.
[2]Space Science Laboratory, University of California, Berkeley, California, USA.
[3]Center for Atmospheric Research, University of Massachusetts, Lowell, Massachusetts, USA.

0148-0227/11/2011JA016733

disruption of the adiabatic particle motion resulting from the distortions of the magnetic field during the large storms (which increases the field line curvature) can cause a loss of the trapped protons [*Hudson et al.*, 1997; *Young et al.*, 2008]. According to the HEO-3 observations, *Selesnick et al.* [2010] found that the time-dependent geomagnetic cutoff suppression could be the cause of significant losses.

[5] However some key questions still remain: What is the response of higher energy protons (35–500 MeV) in the inner radiation belt to the large magnetic storms? Are the responses of the higher energy protons to the storms also energy independent? Answers to these questions can help us to understand the physical processes that occur in the inner radiation belt during geomagnetic storms. In this work we present observations of higher energy protons in three energy ranges (35–70 MeV, 70–140 MeV and 140–500 MeV) measured by detectors on three NOAA POES satellites during the years 1998–2005. We have studied the responses of the high-energy protons in the inner radiation belt (L = 1 to 3) and have compared the features to the model predictions of the curvature induced scattering loss mechanism. We also compared the observations of NOAA POES and HEO-3 and discussed other possible mechanisms for the observed additional proton losses.

2. Data Selection

[6] The primary data used in this work come from the P7, P8 and P9 omni-directional detectors of the MEPED (Medium Energy Proton Electron Detector) instruments onboard NOAA15, 16 and 17 satellites. NOAA15 and NOAA17 are 'AM' satellites (dayside local time crossing is about 10:00), launched into an 810 km circular polar orbit in May 1998 and June 2002 respectively. On the other hand, NOAA16 is a 'PM' satellite (dayside local time crossing is about 13:30) and was launched into a circular orbit in September 2000. The orbit of NOAA16 is about 40 km higher than NOAA15 and NOAA17. Each omni-directional sensor consists of a silicon surface-barrier, solid-state detector, 3 mm thick, with a 50 mm^2 sensitive area. The P7 detector is masked by a 2.13 mm thick Cu (Copper) shell, subtending 120° field of view, and sets the minimum proton energy at 35 MeV. This detector also responds to electrons >6 MeV. The P8 detector is masked by a 4.57 mm thick W (tungsten) shell, subtending 180° field of view, and sets the minimum proton energy at 70 MeV. The P9 detector is masked by a 14.96 mm thick W, also subtending 180° field of view, which sets the minimum detectable proton energy at 140 MeV. The thick W shells that cover the P8 and P9 detectors prevent relativistic electrons with energies less than 10 MeV from reaching the solid-state detectors [*Evans et al.*, 2008]. The omni-directional detectors are mounted to view radially outward from the Earth. The proton fluxes in three energy ranges of 35–70 MeV, 70–140 MeV and 140–500 MeV can be calculated from the counts of the P7, P8 and P9 detectors [*Evans and Greer*, 2004]. In order to place the observation of NOAA POES satellites into the geomagnetic storm context, we have also used the Dst index from the National Geophysical Data Center (http://spidr.ngdc.noaa.gov/spidr/).

3. Observations of NOAA POES Satellites

[7] The differential fluxes of 35–70 MeV, 70–140 MeV and 140–500 MeV protons from NOAA15, 16 and 17 satellites are shown as a function of L and Universal Time (Figures 1–3). The measurements cover the time periods 1998–2004 (NOAA15), 2001–2005 (NOAA 16) and 2002–2005 (NOAA17). The trapped protons in the inner radiation belt are peaked around L = 1.3–1.5 and are visible below the region L < 2.5. NOAA satellites sampled the South Atlantic Anomaly region, where the trapped protons can be observed at low altitudes, with roughly 12-h resolution (as the rotation of the Earth brings these longitudes under the ascending and descending legs of the spacecraft's polar orbit). Hence, the detectors cannot pinpoint timing of changes with a resolution of better than one-half day. The data have been averaged over 1 day and L intervals of 0.1. The L values were obtained from the IGRF model [*Maus et al.*, 2005] using the McIlwain formulation [*Roederer*, 1970].

[8] Significant variations of the trapped 35–70 MeV proton flux in the outer region of the inner radiation belt are clearly visible in Figure 1, which is similar to the variations of 27–45 MeV protons measured by HEO-3 [*Selesnick et al.*, 2010]. From the observations of NOAA15 during 1998–2005 (Figure 1, top), we have identified 7 loss events, satisfying the condition of a clear rapid (~1 day) decrease in the L < 2.5 trapped proton fluxes. The number of the loss events identified from NOAA data is less than that identified from HEO-3 data. A possible reason is the difference in the energy range. Comparing Figures 1–3, we see a clear tendency that as the proton energy increases, fewer number of loss events can be identified in the data. In Figure 3, only weak variations can be seen from the data of 140–500 MeV protons during several large storms since these energies are absent from the outer portion of the inner belt where the losses occur.

[9] To further investigate the loss events, the proton fluxes before and after each loss event at different L shells have been averaged over separate periods before and after each event during which the fluxes did not change significantly. Figure 4 shows the proton fluxes before and after the seven loss events identified from the data of three NOAA satellites. The day intervals of the loss events are also shown. For example, for event 7, the day interval is 313–314 in 2004. The average fluxes before event 7 were computed from the data between day 310 and 312 in 2004, while for the fluxes after event 7 they were computed from days 315 and 318 in 2004. Also listed is the minimum value of the Dst during the events. Different color shows the proton fluxes for different energy channels. It can be seen that the same event measured by different NOAA satellites shows the same features.

[10] From Figure 4, we can summarize some features of the loss events measured by the NOAA satellites: (1) The responses of the three energy channels to the storms are different. The fluxes of 35–70 MeV proton show a clear decrease in the outer region of the inner radiation belt for the large storms with the minimum Dst < −200 nT; only storms with minimum Dst < −350 nT can cause a clear decrease in the fluxes of 70–140 MeV proton, such as events 3, 4, 5 and 7, while only small effects are seen in the fluxes of 140–500 MeV protons. Therefore, the loss events measured by the NOAA satellites are energy dependent. (2) After event 2 and event 4, the proton fluxes of the lower two energy channels in the region of L > 2.4 ~ 2.5 show a large increase, which are caused by injections during the storms. (3) The whole proton

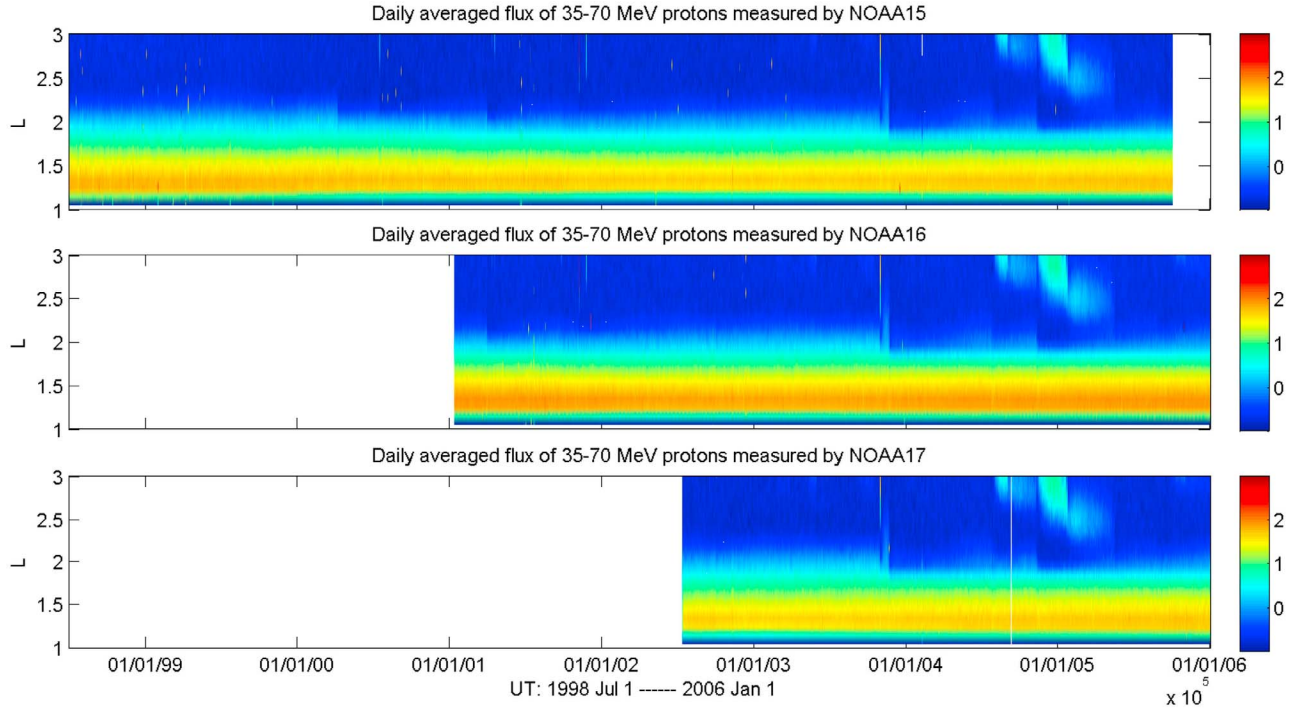

Figure 1. Color-coded 35–70 MeV proton differential fluxes as a function of L and Universal Time from (top) NOAA15, (middle) NOAA16, and (bottom) NOAA17. Data have been averaged over 1 day and 0.1 L bins. White areas represent data gaps. The flux unit is protons/cm^2/s/sr. The colors show the logarithm of the proton flux. The flux enhancement in the region of L > 2.3 from late 2004 to early 2005 could be the high energy electron contamination.

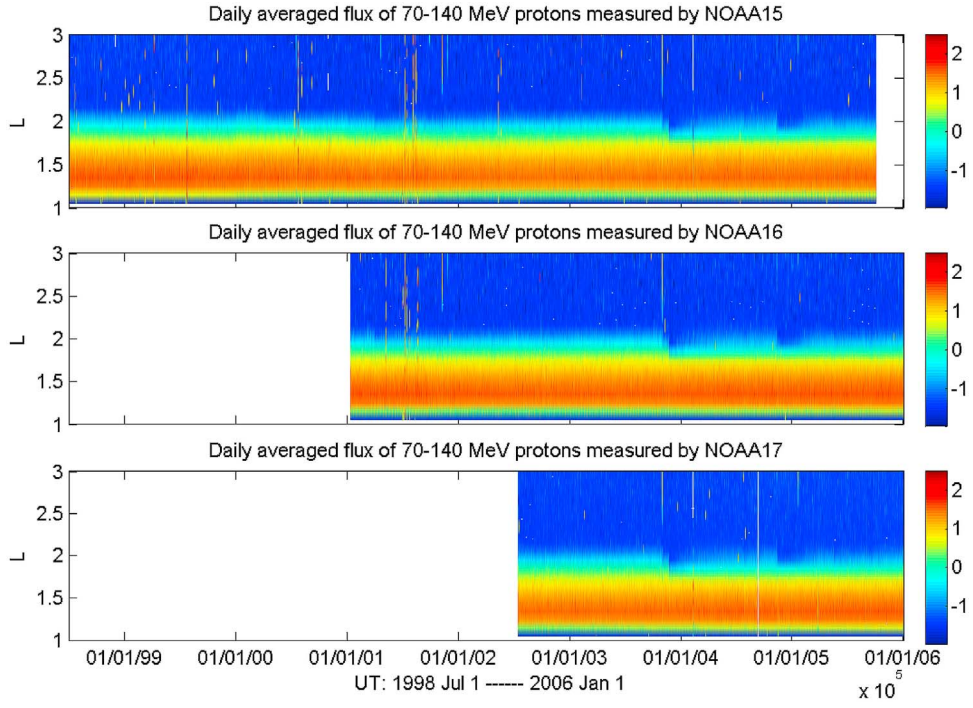

Figure 2. Color-coded 70–140 MeV proton differential flux as a function of L and Universal Time from (top) NOAA15, (middle) NOAA16, and (bottom) NOAA17. Data are averaged over 1 day and 0.1 L bins. White areas represent data gaps. The flux unit is protons/cm^2/s/sr. The colors show the logarithm of the proton flux.

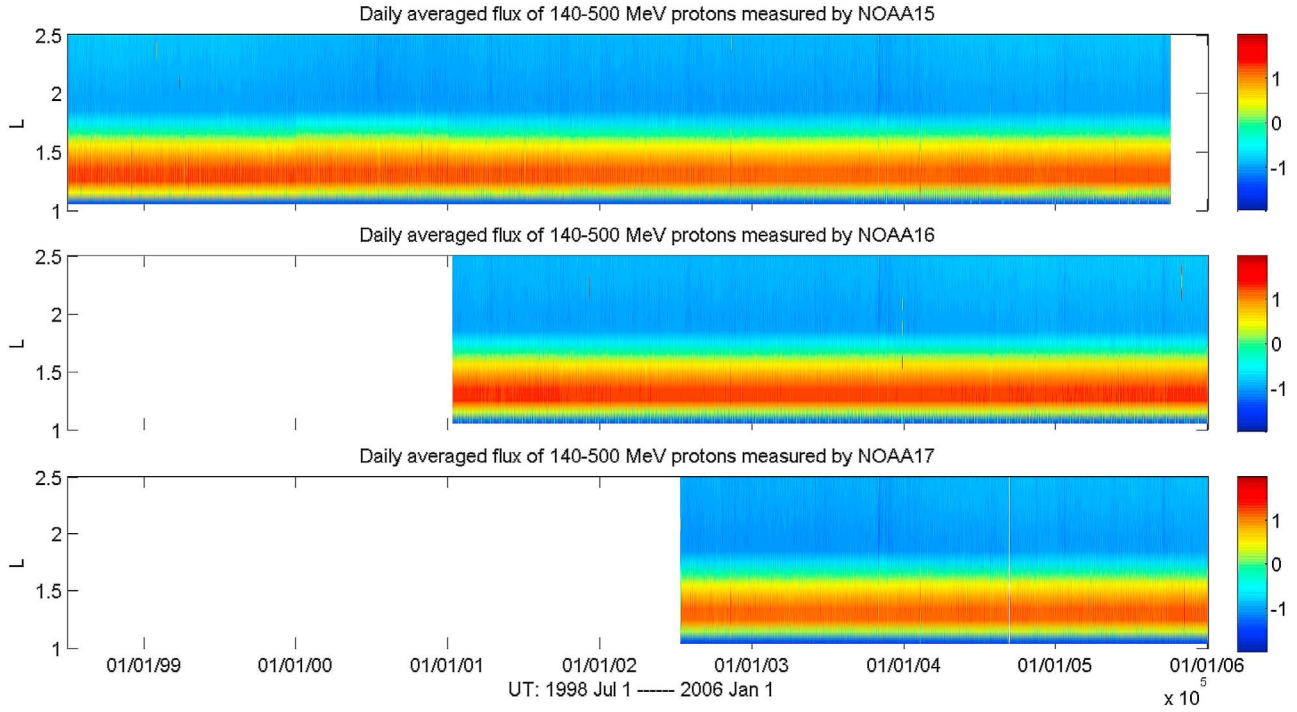

Figure 3. Color-coded 140–500 MeV proton differential flux as a function of L and Universal Time from (top) NOAA15, (middle) NOAA16, and (bottom) NOAA17. Data are averaged over 1 day and 0.1 L bins. White areas represent data gaps. The flux unit is protons/cm^2/s/sr. The colors show the logarithm of the proton flux.

flux curves below L = 1.7 after the loss events did not show a horizontal shift to lower L shell regions. Therefore, the decrease of the proton fluxes in the outer region of the inner radiation belt is not caused by the inward transport of the inner radiation belt protons, which is in agreement with the conclusions from HEO-3 [*Selesnick et al.*, 2010].

4. Theoretical Analysis and Simulation

[11] Magnetic storms could result in decrease of the radiation belt proton fluxes in the region L = 2 ~ 3, where injections occur [*Lorentzen et al.*, 2002]. These loss events during the large storms have been attributed to disruption of the adiabatic particle motion due to distortion of the magnetic field [*Hudson et al.*, 1997]. A particular type of distortion is due to the increase of the field line curvature [*Young et al.*, 2008] that causes a breakdown of the first adiabatic invariant of the particles trapped in the radiation belt. This can lead to pitch angle scattering of the particles. The onset of field line curvature scattering is related to the adiabaticity parameter $\varepsilon = r_g/r_c$, where $r_g = p/(qB_0)$ is the gyroradius of the particle, p is momentum, q is the electric charge, B_0 is the equatorial field magnitude and r_c is the radius of curvature of the field line at $B = B_0$. The scattering threshold for the particle populations near the edge of the loss cone is $\varepsilon = 0.1$ [*Imhof et al.*, 1997; *Young et al.*, 2008].

[12] *Selesnick et al.* [2010] used the threshold $\varepsilon = 0.1$ and simulated the loss event caused by the field line curvature scattering with the TS04c model [*Tsyganenko and Sitnov*, 2005], which is a static storm-time magnetic field model. Comparison of the simulation results with observations by HEO-3 satellite found the reduced fluxes occurred at the L-values significantly larger than the L-values of the observed reductions. The simulation results also found a much steeper gradient in L than the observed exponential decrease. Most importantly, the simulation results did show energy dependence in the location of the decrease, which could not be found in the HEO-3 data. Since the highest lower energy threshold of HEO-3 observations and the corresponding simulations is 27 MeV, it is not clear if the field line curvature scattering mechanism has an effect on the higher energy protons during geomagnetic storms.

[13] The parameter ε varies with particle energy, equatorial magnetic field strength B_0 and curvature of the field line at B_0. For the case of quiet time simulated by *Selesnick et al.* [2010], B_0 decreased with the increase of L shell, and thus the gyroradius also increased for the particles with the same energy. However, the curvature radius of the field line at B_0 also increased with the L shell (the quiet time curve), so a further study is needed to show how ε varied with L shell.

[14] To see how ε varies with L shell, we have calculated the geomagnetic field with the TS04c model, which reproduced very well the Dst variations during the large storms from 1998 to 2002. Figure 5 shows the L-shell variations of the equatorial geomagnetic field strength B_0 and the radius of curvature of the field line at B_0 at midnight. The variations are for the time of the minimum Dst associated with event 7 as shown in Figure 4. Event 7 was chosen because there was a clear loss of protons in the energy channels 35–70 MeV and 70–140 MeV (NOAA15–17 satellites). Model predictions show for large storms, there is a decrease of B_0

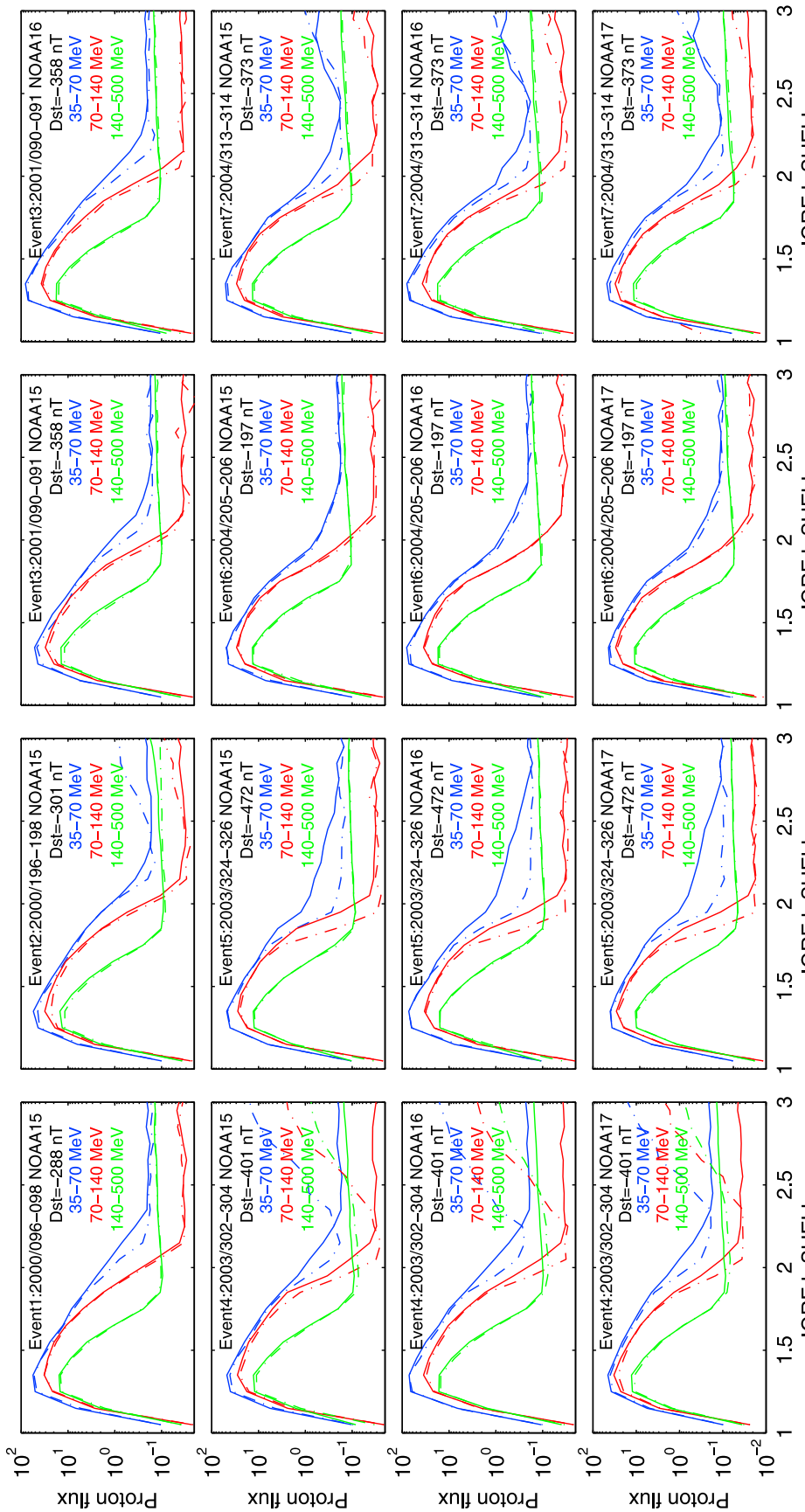

Figure 4. Binned average proton fluxes versus L before (solid line) and after (dash-dot lines) each of seven events. The panels show 7 events from NOAA15 data (Events 1–7), 5 events from NOAA16 data (Events 3–7) and 4 events from NOAA17 data (Events 4–7). The 35–70 MeV, 70–140 MeV and 140–500 MeV protons are shown by blue, red and green colors respectively. Each event includes the event number, year, day interval, NOAA satellite ID and the minimum Dst (nT) during the event.

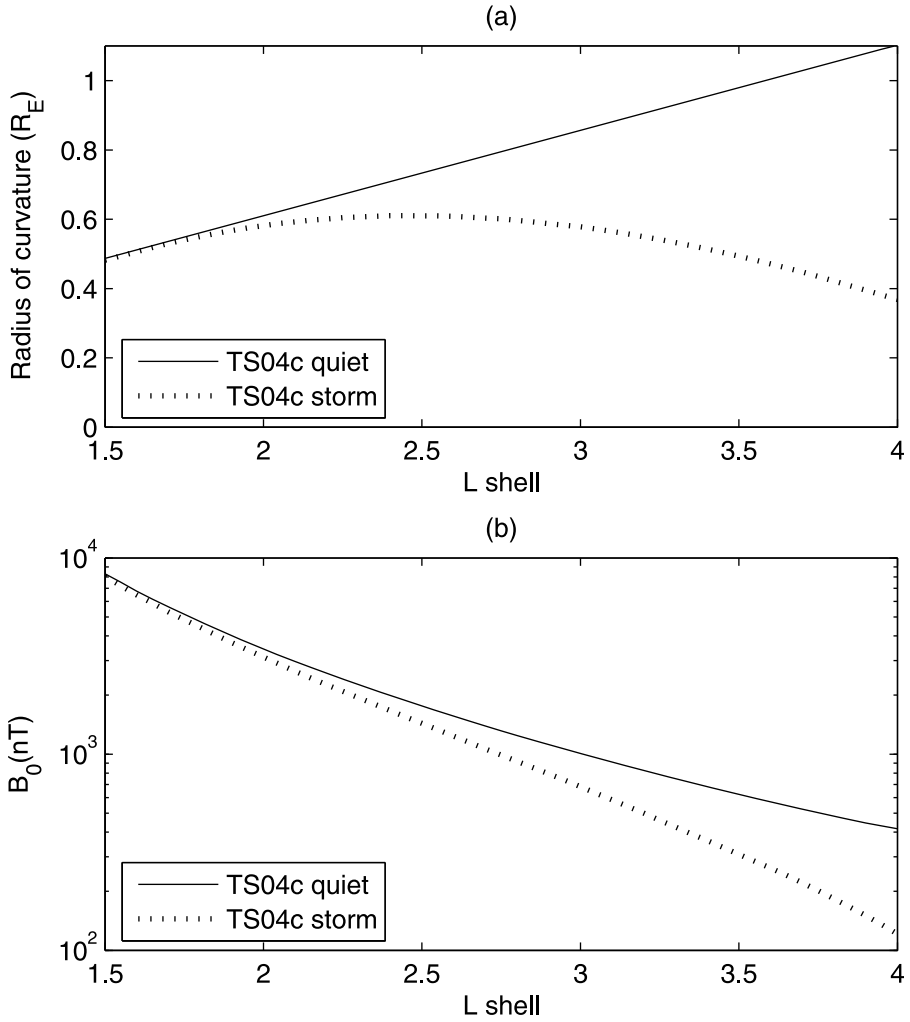

Figure 5. (a) Radii of curvature of the geomagnetic field line at midnight and at B_0, calculated using the quiet time TS04c model (solid line) and the most disturbed TS04c model during event 7 (dotted line). (b) Equatorial geomagnetic field strength calculated using the quiet time and disturbed models at midnight.

and radius of curvature of the field line at B_0, especially for large L shells.

[15] Figure 6 shows ε as a function of L for the four threshold energies (35, 70 140 500 MeV) of the three proton channels for the quiet and storm cases. We can see that ε for these protons increases with L. The threshold for scattering (or trapping limit) of ε (ε = 0.1) are shown as horizontal dashed lines. The cross point of the ε - L curve and the horizontal dashed line shows the critical L shell of the field line curvature scattering (line L_{cs}) for protons decreases with increasing threshold energy. Thus, the protons in the region of $L \geq L_{cs}$ will be lost due to field line curvature scattering, while the protons in the region of $L < L_{cs}$ will be trapped.

[16] To further clarify the variation of L_{cs} with proton energy, we have calculated the critical L shell of the field line curvature scattering for proton energies from 15 MeV to 500 MeV (the energy step is 1 MeV) for both quiet and storm cases, based on the geomagnetic field parameters shown in Figure 5. Figure 7 shows the behavior of L_{cs} as a function of proton energy. The L_{cs}s for the proton with energy larger than 320 MeV are smaller than 1.5, the lower limit of the L range for the geomagnetic field parameters in our calculation.

[17] From Figures 6 and 7, we can see some interesting features: (1) Comparing the critical L shell of the field line curvature scattering for protons with different threshold energy, it is found that L_{cs} decreases with the increase of the proton energy, suggesting that protons with higher energy are more unstable than those with lower energy at the same L shell. This implies that the fluxes in the outer region of the inner radiation belt for the three proton channels 35–70 MeV, 70–140 MeV and 140–500 MeV were mainly detecting protons with energies close to the lower energy threshold of each channel. Figure 8 compares L_{cs} values calculated by the quiet time TS04c model for the proton energies of 27, 35, 70 and 140 MeV with the quiet time outer boundaries of the inner radiation belt for three NOAA proton channels and one HEO-3 proton channel (27–45 MeV), which are determined by the L shells where the proton fluxes change from the exponential variation to a constant background value (Figure 4). The outer boundary of each channel is at the L shell of the cross point between

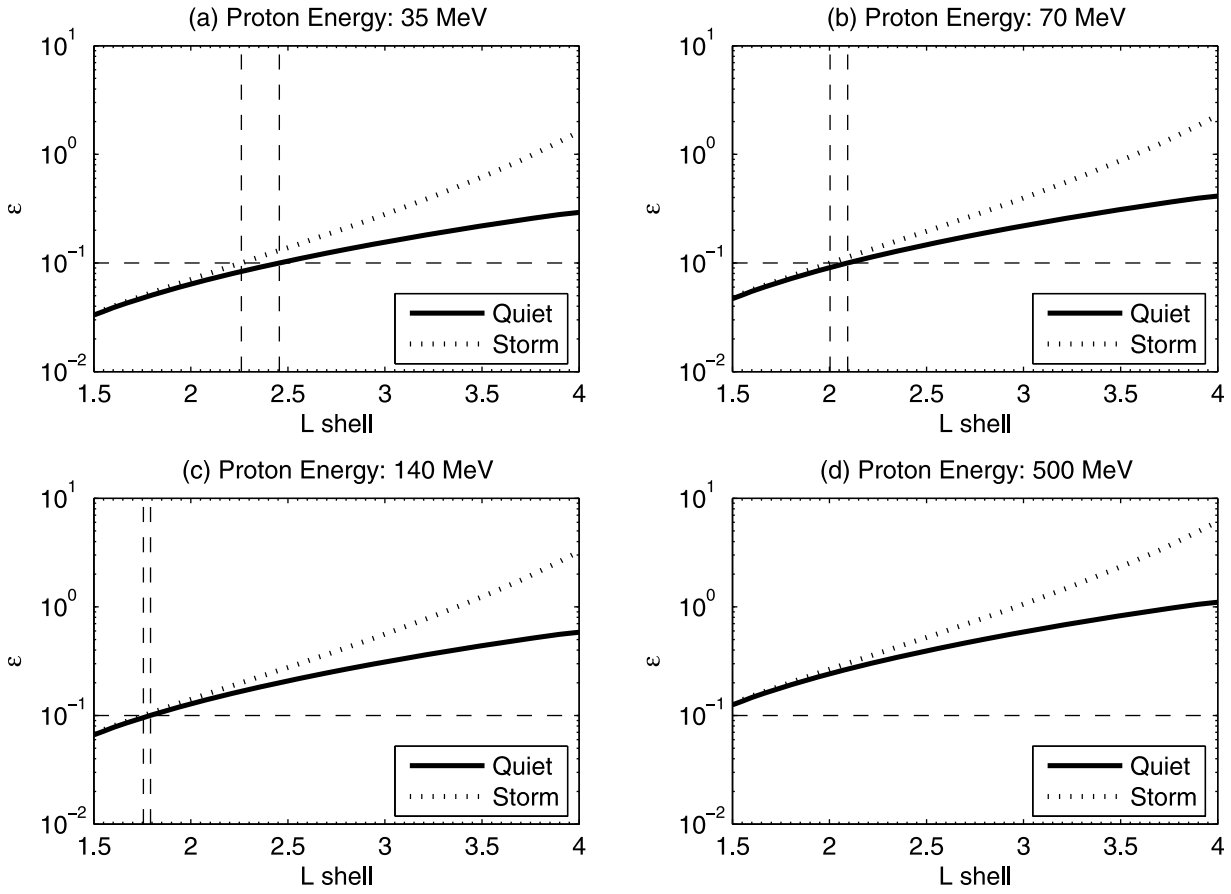

Figure 6. The adiabaticity parameter ε as a function of L for four threshold energies of the three proton channels. (a–d) Calculated results for 35 MeV, 70 MeV, 140 MeV and 500 MeV protons, respectively. The solid curve is the quiet case and the dotted curve is for the storm case. The horizontal dashed line shows the scattering threshold (or the trapping limit) of ε. The vertical dashed lines show the critical L shell of the field-line curvature scattering for the quiet and storm cases.

the fitted exponential variation curve of the inner belt flux and the fitted linear line of the background flux at larger L shells. We see here that the outer boundaries derived from the three NOAA proton channels are in good agreement with the L_{cs}s calculated by the model for the proton energies of 35, 70 and 140 MeV. The outer boundary of the 27–45 MeV proton measured by HEO-3 is slightly larger than the L_{cs} calculated by the model for the proton energy of 27 MeV. The larger L shell of the outer boundary of HEO-3 observation may be caused by other physical processes, such as injection. It is clear that the distribution of the protons in the inner radiation belt is affected by the field-line curvature scattering as has long been understood [*Hastie et al.*, 1967; *Il'in et al.*, 1986; *Delcourt et al.*, 1996; *Anderson et al.*, 1997; *Hudson et al.*, 1998; *Young et al.*, 2002, 2008]. (2) The distortion of the geomagnetic field during the large storm causes an increase of ε for at all L shells, which leads to an inward movement of L_{cs}. The inward movement of the outer boundary is larger for the lower energy channels, which results in much more loss of the lower energy protons. Therefore some aspects of the energy dependence of the loss events measured by three NOAA satellites can be explained by the field-line curvature scattering.

[18] A modeling of the loss event measured by NOAA satellite is made based on the L shell distribution of the proton spectrum predicted by AP8 model [*Sawyer and Vette*, 1976] and the trapping limit of the adiabaticity parameter ε. In the calculation (1) we first calculate the average differential flux at 800 km (the orbit altitude of NOAA satellites) at different L shell (from L = 1.6 to L = 2.5) for protons in the energy range 30 to 500 MeV under solar maximum condition. The resolutions of energy and L shell are $\Delta E = 1$ MeV and $\Delta L = 0.1$ respectively. (2) At each L shell, we calculate ε for all energies with the geomagnetic field parameters as shown in Figure 5. (3) We assume that all of the protons with $\varepsilon > 0.1$ will be lost due to the field line curvature scattering, and then we obtain the integrated flux for the corresponding proton channels of NOAA satellites at each L shell.

[19] Figure 9 shows event 7 measured by NOAA15 and NOAA17 and the modeling results for this event. For the quiet time, the predictions of three proton channels by AP8 model fit the NOAA measurements well in the outer region of the inner radiation belt while large deviations are observed in the region close to the center of the inner radiation belt. It should be noted that the data used to develop AP8 model were mainly measured before 1980s. The inner radiation belt has undergone a large variation after

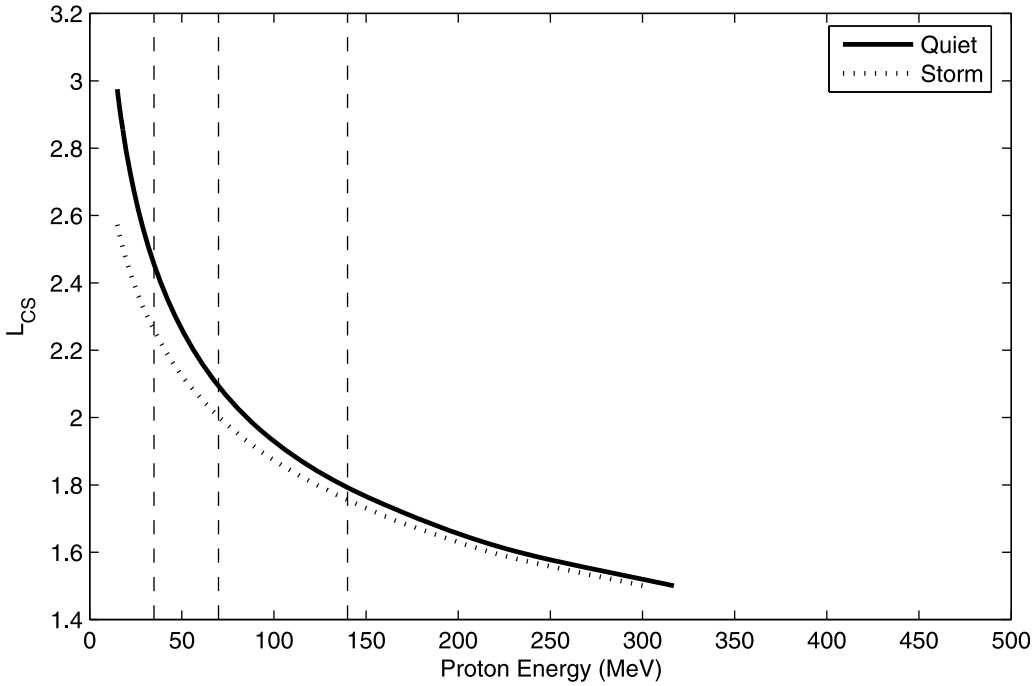

Figure 7. Variations of L_{cs} (the critical L shell of the field line curvature scattering) for proton energies from 15 MeV to 500 MeV for both quiet (solid line) and storm (dotted line) cases. The dashed lines indicate the proton energies of 35 MeV, 70 MeV and 140 MeV.

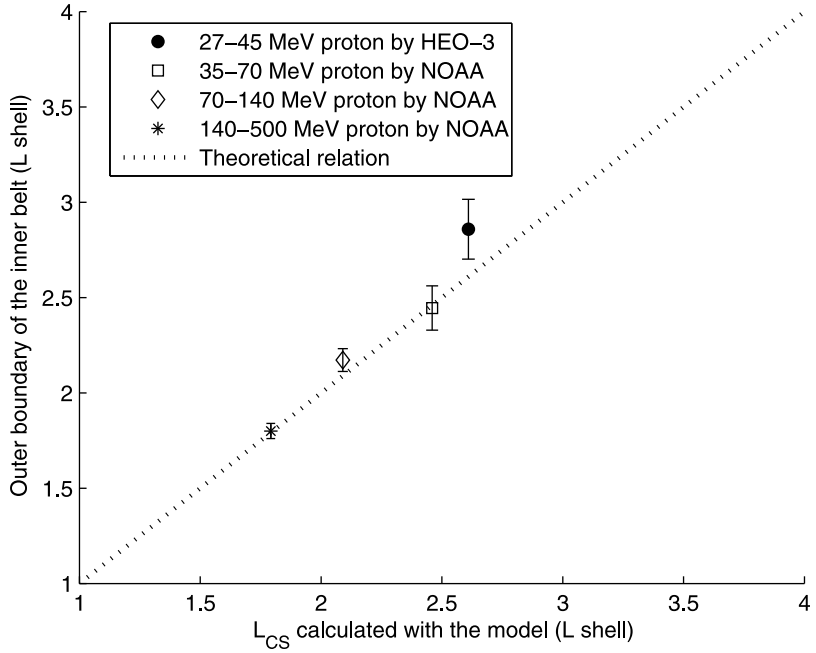

Figure 8. Relationship between the L_{cs}s calculated by the quiet time TS04c model for the proton energies of 27 (the dot), 35 (the square), 70 (the diamond) and 140 MeV (the star) and the quiet time outer boundaries of the inner radiation belt for three NOAA POES proton channels (35–70 MeV, 70–140 MeV and 140–500 MeV) and one HEO-3 proton channel (27–45 MeV). The error bars show the standard deviations of the outer boundaries derived from the NOAA and HEO-3 data. The dotted line shows an ideal relation between them. The HEO-3 data are from *Selesnick et al.* [2010].

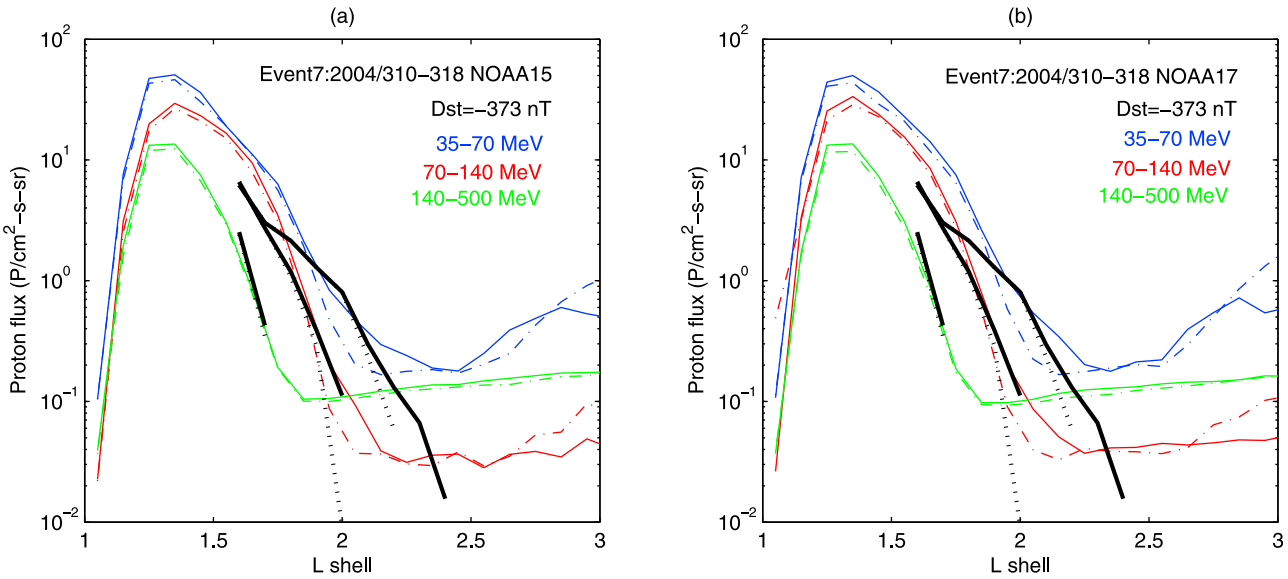

Figure 9. Comparison of the event 7 measured by (a) NOAA15 and (b) NOAA17 and the modeling results based on AP8 model and trapping limit of the adiabaticity parameter ε. The data of 35–70 MeV, 70–140 MeV and 140–500 MeV protons are shown by the lines with blue, red and green colors respectively. The binned average proton fluxes versus L before and after event 7 are shown with the solid and dash-dot lines with colors. The black lines show the modeling results. The thick black solid lines show the original proton flux predicted by AP8 model for the corresponding proton channels, and the black dotted lines show the proton flux, excluding the protons with $\varepsilon > 0.1$.

almost three decades caused by the long-term evolution of the geomagnetic field, such as the northwest drift of Southern Atlantic Anomaly (SAA) [*Heynderickx*, 1996; *Pu et al.*, 2005]. Therefore the long-term variations of the inner radiation belt are a possible reason for the deviations in the region close to the center of the inner radiation belt. However, the loss event occurs only in the outer region of the inner radiation belt, so the deviations of the proton fluxes near the center of the inner radiation belt do not affect our study. For the storm time modeling, we can see that the proton losses in the outer region of the inner radiation belt are well reproduced by the field line curvature scattering mechanism for the 70–140 MeV and 140–500 MeV channels, but not for the 35–70 MeV channel.

5. Discussion

[20] The proton loss events measured by three NOAA satellites have provided an excellent opportunity to investigate the physics of the inner radiation belt. Previous studies have shown that the pitch angle scattering induced by the geomagnetic field line curvature is an important loss mechanism for the protons in the inner radiation belt [*Hastie et al.*, 1967; *Chirikov*, 1987; *Birmingham*, 1984; *Delcourt et al.*, 1996; *Young et al.*, 2002]. According to the theoretical analysis, the outer boundaries of three proton channels measured by NOAA satellites during the quiet time are in good agreement with the quiet time critical L shells calculated with the field line curvature scattering. This observation suggests that the field line curvature scattering is probably the main controller of the static proton distribution in the inner radiation belt.

[21] The distribution of the inner radiation belt protons measured by NOAA satellites after the large geomagnetic storms shows that the local maximum flux of the trapped protons was not transported inward, which agrees with the HEO-3 observations [*Selesnick et al.*, 2010]. Therefore the proton flux decrease in the outer region of the inner radiation belt after large storms represents a true loss. The modeling result of the storm-time geomagnetic field model shows that large storms have little effect on the geomagnetic field of the inner magnetosphere ($L < 2$), but leads to a large distortion in the outer magnetosphere ($L > 2$). The decreasing equatorial magnetic field strength and the curvature radius lead to an exponential increase of the adiabaticity parameter ε as shown in Figure 6. Furthermore, the field line curvature scattering is dependent on ε and the protons at higher L are thus more strongly affected by field-line curvature scattering. Therefore the flux of the protons in the outer region of the inner radiation belt should abruptly decrease and result in a loss event. Figures 4 and 9 confirm that the proton fluxes decrease exponentially near the outer boundaries of the inner radiation belt.

[22] The loss event 7 measured by NOAA15 and NOAA17 simulated with the radiation belt model (AP8) and the storm time geomagnetic field model (TS04c) shows that the trapping limit of the adiabaticity parameter ε can explain the losses of the 70–140 MeV and the lack of losses in 140–500 MeV proton channels. However the simulation model cannot account for the observed reduction in the proton flux of 35–70 MeV. *Selesnick et al.* [2010] also found that the loss of 27–45 MeV proton due to the field line curvature scattering cannot explain the more intensive

loss observed near the region of L = 2. In fact, from Figure 4, it can be seen that the inner extents of the proton losses in the two lower energy channels (35–70 MeV and 70–140 MeV) in event 3, 4, 5 and 7 are almost at the same L shell, which are similar to the HEO-3 observations in low energy proton channels. Furthermore, in event 1, only the 35–70 MeV proton channel has a clear loss. These observations and the simulations imply that the additional loss due to other mechanisms may exist especially for the lower energy protons. One possible reason for the additional loss is related to the third adiabatic invariant of the trapped protons [*Selesnick et al.*, 2010]. From Figure 5, it can be seen that the equatorial magnitude of the geomagnetic field, B_0, decreases during large geomagnetic storms, which leads to a decrease of the magnetic flux within the drift orbit of the trapped protons. To conserve the third adiabatic invariant, the trapped protons will move radially outward into regions of weaker magnetic field. As we know, the proton with a certain energy is easier to be lost due to the field line curvature scattering at larger L shells. Therefore the outward motion related to the third adiabatic invariant can cause the additional loss of the trapped protons. It also can be seen from Figure 5 that the decrease of the geomagnetic field magnitude is much larger at large L shells, where the lower energy protons are trapped. So the additional loss related to the third adiabatic invariant is prominent for the lower energy protons.

[23] *Looper et al.* [2005] presented that the EUV-inflated atmosphere after the associated solar flares could be a possible mechanism for the 'dropout' of the inner belt protons observed by SAMPEX. The enhanced EUV flux heats the entire dayside atmosphere and the flux of the trapped protons at all L shells in the inner belt should be affected. However, according to the observations of HEO-3 and NOAA POES, the proton loss just occurs close to the outer boundary of the inner belt. Therefore, the EUV-inflated atmosphere could not be the main cause of the proton loss observed by NOAA POES and HEO-3.

[24] Comparing the observations of HEO-3 and NOAA POES, we can find an interesting feature of the loss events. There are fewer loss events in the NOAA POES data than in the HEO-3 data. One possible reason is the energy dependence of the field line curvature scattering. From Figure 7, it's clear that the critical L shells for most of the proton energies (35–320 MeV) move inward during storms and the inward movement is larger as the proton energy decreases. This implies there is more loss in the lower energy channels. From Figures 1–3, we can see this trend with energy. The other possible reason may be the different orbits of NOAA POES and HEO-3. HEO-3 is in a highly elliptical orbit (Molniya orbit), with a 12-h period, perigee at few hundred kilometers, apogee at roughly 7 Re, and inclination of about 63°. NOAA POES is in a polar orbit at 800 km and the inclination is about 98°. So the loss events observed by HEO-3 are closer to the geomagnetic equator than those observed by NOAA POES since the detectors onboard NOAA POES (at 800 km) measure those protons with small equatorial pitch angles (the trapped inner belt protons with large equatorial pitch angles are mirrored back before they can reach 800 km). On the other hand, HEO-3 can measure the trapped protons within a larger equatorial pitch angle range. If the loss just occurs for the protons with larger equatorial pitch angles, HEO-3 would measure the loss event, but NOAA POES will not. However, NOAA POES orbit has its advantages. NOAA POES orbit can measure the proton distributions at all L shells in the inner belt, but the data in the region of L < 1.7 or L < 2.0 (for some time periods) are missed by HEO-3. NOAA POES orbit also simplifies the simulation of the field line curvature scattering. Because of the small equatorial pitch angles of the proton measurements of NOAA POES, the corresponding limit of the adiabaticity parameter ε can be assumed to be a constant, $\varepsilon = 0.1$ [*Selesnick et al.*, 2010]. Therefore it is not necessary to consider the different losses at different pitch angles in the simulation.

[25] Another interesting observation is the recovery time of the loss events. According to the measurements of NOAA and HEO-3 satellites, it takes several months for the protons in the outer region of the inner radiation belt to recover. The long time scale of the recovery suggests that the physical processes controlling the trapped protons in the inner radiation belt involve the outward radial diffusion.

6. Conclusion

[26] The responses of the high-energy protons (35–70 MeV, 70–140 MeV and 140–500 MeV) below L = 3 to the large magnetic storms (|Dst| > 200 nT) during 1998 to 2005 have been investigated with the measurements by three NOAA POES satellites. It is found that the loss events observed by NOAA satellites show the energy dependence. The pitch angle scattering mechanism induced by the increasing field line curvature has been examined to understand the loss event and its energy dependence during the large magnetic storms. According to the theoretical analysis and the modeling results based on the storm-time TS04c and AP8 models, the distribution of the high-energy protons during the quiet time and the loss events during the large storms both can be explained by the trapping limit of the field line curvature scattering mechanism, especially for the higher two energy channels (70–140 MeV and 140–500 MeV) measured by NOAA satellites. The additional proton loss in the lower energy channel (35–70 MeV) could be due to the storm-caused weakening of geomagnetic field combined with L dependent lifetimes induced by curvature scattering.

[27] **Acknowledgments.** We would like to acknowledge the contributions of the MEPED instruments onboard NOAA satellites and the geomagnetic data collection at the National Geophysical Data Center. This work is supported partly by the NSFC grants 40831061 and 41074117. The authors acknowledge R. S. Selesnick for the explanation of the field line curvature scattering and N. A. Tsyganenko for providing the storm time TS04c model.

[28] Masaki Fujimoto thanks the reviewers for their assistance in evaluating this paper.

References

Anderson, B. J., R. B. Decker, and N. P. Paschalidis (1997), Onset of nonadiabatic particle motion in the near-Earth magnetotail, *J. Geophys. Res.*, *102*(A8), 17,553–17,569, doi:10.1029/97JA00798.

Baker, D. N., S. G. Kanekal, T. I. Pulkkinen, and J. B. Blake (1999), Equinoctial and solstitial averages of magnetospheric relativistic electrons: A strong semiannual modulation, *Geophys. Res. Lett.*, *26*, 3193–3196, doi:10.1029/1999GL003638.

Baker, D. N., S. G. Kanekal, R. B. Horne, N. P. Meredith, and S. A. Glauert (2007), Low-altitude measurements of 2–6 MeV electron trapping lifetimes at 1.5 < L < 2.5, *Geophys. Res. Lett.*, *34*, L20110, doi:10.1029/2007GL031007.

Birmingham, T. J. (1984), Pitch angle diffusion in the Jovian magnetodisc, *J. Geophys. Res.*, *89*(A5), 2699–2707, doi:10.1029/JA089iA05p02699.

Blake, J. B., M. S. Gussenhoven, E. G. Mullen, and R. W. Fillius (1992), Identification of an unexpected space radiation hazard, *IEEE Trans. Nucl. Sci.*, *39*, 1761–1764, doi:10.1109/23.211364.

Chirikov, B. V. (1987), Particle dynamics in magnetic traps, in *Reviews of Plasma Physics*, vol. 13, edited by A. B. B. Kadomtsev, pp. 1–91, Consult. Bur., New York.

Delcourt, D. C., J. A. Sauvaud, R. F. Martin Jr., and T. E. Moore (1996), On the nonadiabatic precipitation of ions from the near-Earth plasma sheet, *J. Geophys. Res.*, *101*(A8), 17,409–17,418, doi:10.1029/96JA01006.

Dessler, A., and R. Karplus (1961), Some effects of diamagnetic ring currents on Van Allen radiation, *J. Geophys. Res.*, *66*(8), 2289–2295, doi:10.1029/JZ066i008p02289.

Evans, D. S., and M. S. Greer (2004), Polar orbiting environmental satellite space experiment monitor-2: Instrument descriptions and archive data documentation, *Tech. Memo. version 1.3*, Natl. Oceanic and Atmos. Admin. Space Environ. Cent., Boulder, Colo.

Evans, D., H. Garrett, I. Jun, R. Evans, and J. Chow (2008), Long-term observations of the trapped high-energy proton population (L < 4) by the NOAA Polar Orbiting Environmental Satellites (POES), *Adv. Space Res.*, *41*, 1261–1268, doi:10.1016/j.asr.2007.11.028.

Hastie, R. J., J. B. Taylor, and F. A. Haas (1967), Adiabatic invariants and the equilibrium of magnetically trapped particles, *Ann. Phys.*, *41*, 302–338, doi:10.1016/0003-4916(67)90237-0.

Heynderickx, D. (1996), Comparison between methods to compensate for the secular motion of the South Atlantic Anomaly, *Radiat. Meas.*, *26*(3), 369–373, doi:10.1016/1350-4487(96)00056-X.

Hudson, M. K., S. R. Elkington, J. G. Lyon, V. A. Marchenko, I. Roth, M. Temerin, J. B. Blake, M. S. Gussenhoven, and J. R. Wygant (1997), Simulations of proton radiation belt formation during storm sudden commencements, *J. Geophys. Res.*, *102*(A7), 14,087–14,102.

Hudson, M. K., V. K. Marchenko, I. Roth, M. Temerin, J. B. Blake, and M. S. Gussenhoven (1998), Radiation belt formation during storm sudden commencements and loss during main phase, *Adv. Space Res.*, *21*, 597–607, doi:10.1016/S0273-1177(97)00969-1.

Il'in, V. D., I. V. Il'ina, and S. N. Kuznetsov (1986), Stochastic instability of charged particles in a geomagnetic trap, *Cosmic Res., Engl. Transl.*, *24*, 75–83.

Imhof, W. L., D. L. Chenette, E. E. Gaines, and J. D. Winningham (1997), Characteristics of electrons at the trapping boundary of the radiation belt, *J. Geophys. Res.*, *102*(A1), 95–104, doi:10.1029/96JA02797.

Kim, H.-J., and A. A. Chan (1997), Fully adiabatic changes in storm-time relativistic electron fluxes, *J. Geophys. Res.*, *102*(A10), 22,107–22,116, doi:10.1029/97JA01814.

Li, X., D. N. Baker, M. Temerin, T. E. Cayton, E. G. D. Reeves, R. A. Christensen, J. B. Blake, M. D. Looper, R. Nakamura, and S. G. Kanekal (1997), Multisatellite observations of the outer zone electron variation during the November 3–4, 1993, magnetic storm, *J. Geophys. Res.*, *102*(A7), 14,123–14,140, doi:10.1029/97JA01101.

Li, X., D. N. Baker, S. G. Kanekal, M. Looper, and M. Temerin (2001), Long term measurements of radiation belt by SAMPEX and their variations, *Geophys. Res. Lett.*, *28*, 3827–3830, doi:10.1029/2001GL013586.

Looper, M. D., J. B. Blake, and R. A. Mewaldt (2005), Response of the inner radiation belt to the violent Sun-Earth connection events of October-November 2003, *Geophys. Res. Lett.*, *32*, L03S06, doi:10.1029/2004GL021502.

Lorentzen, K. R., J. E. Mazur, M. D. Looper, J. F. Fennell, and J. B. Blake (2002), Multisatellite observations of MeV ion injections during storms, *J. Geophys. Res.*, *107*(A9), 1231, doi:10.1029/2001JA000276.

Maus, S., et al. (2005), The 10th-generation international geomagnetic reference field, *Geophys. J. Int.*, *161*, 561–565, doi:10.1111/j.1365-246X.2005.02641.x.

Miyoshi, Y., A. Morioka, T. Obara, H. Misawa, T. Nagai, and Y. Kasahara (2003), Rebuilding process of the outer radiation belt during the November 3, 1993 magnetic storm: NOAA and EXOS-D observations, *J. Geophys. Res.*, *108*(A1), 1004, doi:10.1029/2001JA007542.

Pu, Z. Y., L. Xie, W. X. Jiao, S. Y. Fu, X. H. Fang, Q. G. Zong, and D. Heynderickx (2005), Drift shell tracing and secular variation of inner zone high energy proton environment in the SAA, *Adv. Space Res.*, *36*, 1973–1978, doi:10.1016/j.asr.2004.09.018.

Reeves, G. D., R. H. W. Friedel, R. D. Belian, M. M. Meiet, M. G. Henderson, T. Onsager, H. J. Singer, D. N. Baker, X. Li, and J. B. Blake (1998), The relativistic electron response at geosynchronous orbit during the January 1997 magnetic storm, *J. Geophys. Res.*, *103*(A8), 17,559–17,570, doi:10.1029/97JA03236.

Roederer, J. G. (1970), *Dynamics of Geomagnetically Trapped Radiation*, 166 pp., Springer, New York.

Sawyer, D. M., and J. I. Vette (1976), Trapped particle environment for solar maximum and solar minimum (AP8), *Rep. 76-06*, Natl. Space Sci. Data Cent., Greenbelt, Md.

Selesnick, R. S., M. K. Hudson, and B. T. Kress (2010), Injection and loss of inner radiation belt protons during solar proton events and magnetic storms, *J. Geophys. Res.*, *115*, A08211, doi:10.1029/2010JA015247.

Tsyganenko, N. A., and M. I. Sitnov (2005), Modeling the dynamics of the inner magnetosphere during strong geomagnetic storms, *J. Geophys. Res.*, *110*, A03208, doi:10.1029/2004JA010798.

Young, S. L., R. E. Denton, B. J. Anderson, and M. K. Hudson (2002), Empirical model for μ-scattering caused by field line curvature in a realistic magnetosphere, *J. Geophys. Res.*, *107*(A6), 1069, doi:10.1029/2000JA000294.

Young, S. L., R. E. Denton, B. J. Anderson, and M. K. Hudson (2008), Magnetic field line curvature induced pitch angle diffusion in the inner magnetosphere, *J. Geophys. Res.*, *113*, A03210, doi:10.1029/2006JA012133.

H. F. Chen, Z. Y. Pu, L. Xie, Q. G. Zong, and H. Zou, School of Earth and Space Sciences, Peking University, Beijing 100871, China. (derakzou@yahoo.com.cn)

G. K. Parks, Space Science Laboratory, University of California, Berkeley, CA 94720, USA.